Towards high-precision calculation of electron capture decays

Xavier Mougeot

Applied Radiation and Isotopes 154 (2019) 108884

Contents lists available at ScienceDirect

Applied Radiation and Isotopes

journal homepage: www.elsevier.com/locate/apradiso

Towards high-precision calculation of electron capture decays

X. Mougeot

CEA, LIST, Laboratoire National Henri Becquerel (LNE-LNHB), Bât. 602 PC111, CEA-Saclay, 91191, Gif-sur-Yvette Cedex, France

HIGHLIGHTS

- An improved theoretical model for electron captures is presented.
- Influence of precise atomic energies is explored.
- Influence of radiative correction is explored.
- Influence of the nuclear component is explored.
- Calculations are compared with available precise measurements.

ARTICLE INFO

Keywords:
Electron capture
Theoretical calculations
Nuclear decay data
Radionuclide metrology

ABSTRACT

Based on previous study, the calculation of electron capture decays has been improved by considering a more accurate atomic model with precise atomic energies, and different radiative corrections have been tested. The computer code has been revised in order to greatly speed-up the calculation and has then been coupled with the BetaShape code. The influence of the nuclear component has also been explored using a simple nuclear model. All the calculations are compared with precise measurements available in the literature.

1. Introduction

The LogFT code (LogFT Program, 2001) and (Gove and Martin, 1971) is currently the reference code for electron captures when evaluating nuclear decay data, either within DDEP (Decay Data Evaluation Project) (Kellett and Bersillon, 2017) or the NSDD (Nuclear Structure and Decay Data) network which provides ENSDF (Evaluated Nuclear Structure Data File) evaluations for every existing nucleus (NNDC and Bhat, 2019). In a previous study, the theoretical predictions of the LogFT code were compared to those of a specific model developed at LNE-LNHB (Mougeot, 2018). Our modelling was more complete and more consistent, including several improvements. However, despite significantly improved results for some radionuclides, it was found that this model suffered from a lack of precision in the atomic wave functions used.

Improvements in these predictions are still necessary, as electron capture properties are crucial features when one is evaluating the decay scheme of radionuclides. On the metrology side, pure electron capture radionuclides can be standardized with the liquid scintillation counting technique, the uncertainty of which partly depends on the decay scheme. A precise knowledge of capture probabilities is also pivotal for many applications, e.g. in geo- and cosmo-chronology for rocks and fossils dating; in the estimate of radiation effects on human tissue at the DNA length scale in nuclear medicine; or for some experiments in fundamental physics which are looking at rare events, in order to evaluate the background components.

In the present study, precise eigenvalues of atomic orbital energies have been considered, and were obtained for atoms from H to U based on a relativistic self-consistent model with an approximate account of the electron correlations. Radiative corrections have also been studied with formulations derived for allowed transitions, and the internal bremsstrahlung spectrum from ^{55}Fe decay has been determined. Our code for electron capture calculation has been improved for better computational efficiency, and then implemented within the BetaShape code. Our modelling is described in Section 2.

In Section 3, we compare the predictions from our modelling with precise experimental data available in the literature for different proton numbers Z and different forbiddenness degrees of transitions. Finally, the influence of nuclear structure is considered in Section 4, with a detailed description of the matrix elements, which have been fully derived starting from the recent work performed in the context of beta decays.

E-mail address: xavier.mougeot@cea.fr.

https://doi.org/10.1016/j.apradiso.2019.108884
Received 28 March 2019; Received in revised form 2 July 2019; Accepted 3 September 2019
Available online 03 September 2019

2. Theoretical description of the electron capture transitions

2.1. Overview of the previous modelling

In a previous publication, we detailed the development of a consistent modelling of electron captures based on the formalism of Behrens and Bühring (1982) which calculates allowed and forbidden unique transitions. Several atomic effects were taken into account: *i*) influence of the hole created by the capture process in the atomic structure, by means of first order perturbation theory; *ii*) shake-up and shake-off effects, using Crasemann's work (Crasemann et al., 1979) to determine the probability $P_{m\kappa}$ of producing secondary vacancies in every (m, κ) orbital of the electron cloud; and *iii*) overlap and exchange effects B_{κ_x}, estimated from the approximate treatment from Bahcall (1965) and from the more precise treatment from Vatai (1970). The total decay probability $\lambda_\varepsilon$was then given as the sum of the capture probability of each subshell, labelled by its quantum number κ_x:

$$\lambda_\varepsilon = \frac{G_\beta^2}{2\pi^2} \sum_{\kappa_x} \frac{\pi}{2} n_{\kappa_x} C_{\kappa_x} q_{\kappa_x}^2 \beta_{\kappa_x}^2 B_{\kappa_x} \left(1 + \sum_{m,\kappa} P_{m\kappa}\right) \tag{1}$$

where G_β is the Fermi coupling constant, n_{κ_x} is the relative occupation number, q_{κ_x} is the momentum of the emitted neutrino, β_{κ_x} is the Coulomb amplitude of the captured electron wave function and C_{κ_x} couples the lepton and nucleon wave functions.

For each atomic subshell, the code developed provides capture probability ratios and, for transitions with sufficient energy, capture-to-positron probability ratios. The sum for each shell (L, M, N, etc.) is also given, as well as the total capture-to-positron probability ratio. Uncertainties were estimated by propagation of the uncertainties on the Q-value and the level energies, and by taking into account the difference between results from Bahcall's approach and Vatai's approach.

This modelling was validated by comparison with published measurements of capture probability ratios and capture-to-positron ratios. However, it was not possible to distinguish between the predictions from Bahcall's and Vatai's approaches, an unsatisfactory conclusion as Vatai's approach is based on a more reliable theoretical description.

2.2. Precise atomic energies

In order to have access to the capture probabilities for each atomic subshell and to calculate the different corrections, the relativistic bound wave functions were determined from the model explained in detail in (Mougeot and Bisch, 2014). In this model, an iterative procedure was implemented in order to reach relativistic Dirac-Fock orbital energies from (Desclaux, 1973) by adjusting the strength of the atomic exchange potential. However, particle correlations, an important physical phenomenon in the many-body problem, were not taken into account in Desclaux's work.

In the present work, we have considered more precise atomic orbital energies determined by Kotochigova (Kotochigova et al., 1997). They were obtained in the framework of the density functional theory by means of the relativistic local-density approximation for a point nucleus. In this approach, electron correlations are embedded in an exchange-correlation potential which depends on the local value of the electron density. The correct parameterization of this dependency is of high importance to get realistic values. These orbital energies are available on the NIST website for elements from H to U (NIST, 2009), and can differ from Desclaux's results by an order of magnitude for some of the least bound subshells.

Our algorithm still remains the same, the iterative process converging to different orbital energies. However, our approach has lost consistency for two reasons. The first one is because we have considered a spherical nucleus while Kotochigova (Kotochigova et al., 1997) have considered a point nucleus. Our wave functions are thus more precise than Kotochigova's on this aspect, which is of importance due to the sensitivity of the capture probabilities to the correctness of the wave functions at the nucleus. The second reason is because the Coulomb potential used in our procedure does not take into account any electron correlation. Our wave functions are thus less precise than Kotochigova's because in our modelling electron correlation information is only included in the atomic energies, while it is expected to influence also the spatial behaviour of the wave functions, and hence their overlaps. As capture probabilities are very sensitive to the energetics of the transition, we can expect that the gain obtained by using more precise atomic energies will dominate over the loss due to the inaccuracy of the overlaps involved in the different corrections.

2.3. Radiative corrections

In regular electron capture, the transition energy is shared between the emitted neutrino and the nucleus. In this two-body process, all the energies are well defined. In the radiative capture process, one or more photons are emitted and the transition energy is then shared between at least three particles, which creates the well-known continuous spectrum of internal bremsstrahlung. The emission probability of a single photon through such a process is typically of about 0.01% per capture event. Processes involving more photons can thus be safely ignored. With such a low probability, the question arises about the necessity of considering radiative corrections in electron captures. In fact, their contribution is much more significant when considering capture-to-positron probability ratios because of the beta plus emission. It is also important to remember that our modelling calculates ratios of capture probabilities for subshells, and radiative corrections can be different from one subshell to another.

In addition, very precise radiative corrections are available for beta transitions (Towner and Hardy, 2008), however it is not the case for electron capture decays. It is therefore mandatory to take into account radiative corrections at the same level of precision for both capture and beta plus transitions when considering capture-to-positron probability ratios. Several formalisms can be found in the literature with different assumptions. Unfortunately, the most precise only describe two or three of the inner subshells and are not consistent for both capture and capture-to-positron ratios. We give below an idea of the precision of the radiative corrections for capture ratios, and then we outline the formalism for the capture-to-positron ratios.

We have studied two formulations of the radiative corrections, derived only for allowed transitions: a Coulomb-free theory from (Morrison and Schiff, 1940) and a fully relativistic theory from (Martin and Glauber, 1958). Coulomb-free theory drastically simplifies the modelling of radiative electron capture by neglecting the momentum and the binding energy of the captured electron, as well as the Coulomb field influence. This theory accurately describes internal bremsstrahlung photon spectra in the high energy region. Morrison and Schiff derived the total radiative capture rate ω_{ns} for an electron in an *s* state per K-capture ω_K by integrating over the photon momentum k:

$$\frac{\omega_{ns}}{\omega_K} = \frac{1}{\omega_K} \int_0^{q_{ns}} \frac{\alpha}{\pi} \frac{\beta_{ns}^2}{\beta_K^2} \frac{k(q_{ns} - k)^2}{q_K^2} \mathrm{d}k = \frac{\alpha}{\pi} \frac{\beta_{ns}^2}{\beta_K^2} \frac{q_{ns}^2}{12} \left(\frac{q_{ns}}{q_K}\right)^2 \tag{2}$$

with α the fine structure constant. One should note that for *s* orbitals, the Coulomb amplitude of the wave function is exactly the value of the wave function at the origin, i.e. $\beta_{ns} = \Psi_{ns}(0)$, and is thus still defined in the context of Coulomb-free theory. Fully relativistic theory leads to much more complicated formulas because of the inclusion of the Coulomb field, even considering analytical relativistic electron wave functions. These formulas are available for some of the most bound orbitals. In the case of a 1*s* captured electron, the energy spectrum of photons from internal bremsstrahlung becomes:

$$\frac{\mathrm{d}\omega_{1s}}{\omega_K} = \frac{\alpha}{\pi} \frac{k(q_{1s} - k)^2}{q_K^2} R_{1s} \mathrm{d}k \tag{3}$$

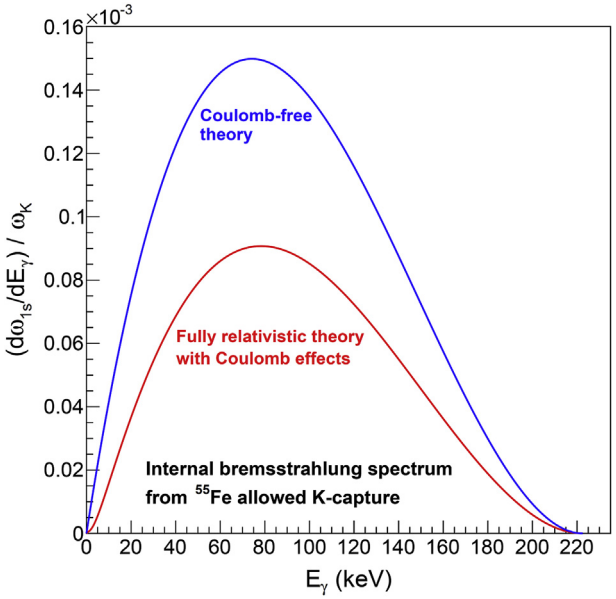

Fig. 1. Internal bremsstrahlung spectrum from ^{55}Fe allowed K capture. The blue spectrum has been calculated using Coulomb-free theory (Morrison and Schiff, 1940). The red spectrum has been calculated by means of the fully relativistic theory from (Martin and Glauber, 1958). (For interpretation of the references to colour in this figure legend, the reader is referred to the Web version of this article.)

with:

$$R_{1s} = \frac{1}{2}(A_{1s}^2 + B_{1s}^2) \tag{4}$$

The quantities $A_{1s}(k)$ and $B_{1s}(k)$ are very complicated integrals which can only be obtained numerically (Bambynek, 1977). We have implemented the procedure established by Intemann (1971) to obtain exact numerical results. We have then applied the Coulomb-free theory and the relativistic theory to the K-capture in the allowed transition of ^{55}Fe decay. This low-energy, ground-state to ground-state transition is very suitable to illustrate the difference between both results. The two energy spectra of internal bremsstrahlung are given in Fig. 1. For Coulomb-free theory, one gets a total radiative capture correction of 0.0037%; for fully relativistic theory, one gets 0.0022%. We can see that the spectrum shape is identical but the total intensity is significantly reduced by taking into account the Coulomb and relativistic effects. However, Coulomb-free theory provides at least the correct order of magnitude of the total radiative correction, even for such a low-energy transition.

Regarding capture-to-positron ratios, we have followed Holstein's formulation (Holstein, 1979) in which the capture part is estimated by Coulomb-free theory and the beta plus part is determined consistently keeping the energy dependent part and omitting the Z dependent parts, as detailed in (Mougeot, 2015). The correction to be applied on the total capture-to-positron ratio is then:

$$\frac{\varepsilon}{\beta^+} \rightarrow \frac{\varepsilon}{\beta^+}(1 + \delta_{r,\varepsilon}) \tag{5}$$

with:

$$\delta_{r,\varepsilon} = \frac{\alpha}{2\pi}\left(3\ln\frac{m_p}{m_e} - \frac{27}{4}\right) + \frac{\alpha}{12\pi}(W_0 + 1)^2 - \langle\delta_\beta\rangle \tag{6}$$

where m_p and m_e are the proton and electron rest masses, $\langle\delta_\beta\rangle$ is the average of the energy-dependent part of the radiative correction applied to the beta plus spectrum, and W_0 is the total energy of the transition. Identical formulation can be derived straightforwardly for the capture-to-positron ratios of n*s* orbitals, e.g. for the K shell:

$$\delta_{r,K} = \frac{\alpha}{2\pi}\left(3\ln\frac{m_p}{m_e} - \frac{27}{4}\right) + \frac{\alpha}{12\pi}q_K^2 - \langle\delta_\beta\rangle \tag{7}$$

In order to avoid inconsistent results between capture probabilities and capture-to-positron probabilities due to the radiative corrections, we chose to consider only Coulomb-free theory in our whole modelling of the electron capture decay. The contribution of the n*s* subshells can be easily subtracted to the total radiative correction:

$$\lambda_\varepsilon\delta_{r,\varepsilon} - \sum_n \delta_{r,ns}\lambda_{ns} = \sum_{\kappa_\chi\neq(ns)} \delta_{r,\kappa_\chi}\lambda_{\kappa_\chi} \tag{8}$$

We then approximate the δ_{r,κ_χ} corrections by an average radiative correction $\delta_{r,\neq ns}$ identical for every other subshell as:

$$\delta_{r,\neq ns} = \left(\lambda_\varepsilon\delta_{r,\varepsilon} - \sum_n \delta_{r,ns}\lambda_{ns}\right) \Big/ \sum_{\kappa_\chi\neq(ns)} \lambda_{\kappa_\chi} \tag{9}$$

Therefore, the radiative corrections applied in our modelling are expected to be overestimated. However, as their absolute contribution is reasonably small, the induced bias should be smaller than the current experimental uncertainties, except for high-precision measurements of low-energy transitions for which a more precise modelling would have to be used.

2.4. Inclusion within the BetaShape code

The BetaShape code has been developed for the last few years to improve the theoretical predictions of beta decays used in nuclear data evaluations (Mougeot, 2017). Electron captures are the other weak-interaction decays of interest in the same context. We have thus implemented the present modelling in BetaShape. However, the calculations are time consuming because of the iterative procedure used to determine the atomic wave functions. In addition, the precise atomic energies from Kotochigova et al. (1997) are only available up to $Z = 92$.

To correct these problems, we have extrapolated the atomic energies of the different orbitals up to $Z = 120$ using their smooth Z dependency. Next, we have neglected the isotope shift of atomic energies, which comes from the nucleus through both a mass effect and a volume effect, because of its small magnitude (Pálffy, 2010). For each Z, we have fixed the mass number A making use of the empirical formula given in (Angeli, 1999) for the number of protons Z_{st} along the stability line:

$$Z_{st} = \frac{A}{1.98 + 0.016A^{2/3}} \tag{10}$$

All the atomic wave functions from $Z = 1$ to $Z = 120$ have then been determined and parameters that depend on the iterative procedure have been tabulated. Eventually, the calculation of electron-capture properties is significantly speeded-up as the iterative procedure is avoided.

The present modelling has been implemented in BetaShape. The program reads the input ENSDF file; determines the transition parameters; calculates each electron capture decay; generates specific output files with detailed information; and updates the ENSDF file with the new values. In addition, the log*ft* value and the splitting of the branch between capture and beta plus transitions are determined for each branch. In a few cases such as ^{205}Pb, K capture is energetically hindered due to a low Q-value compared with the K binding energy. The modelling then calculates all the probability ratios according to the first possible subshell, usually L_1. Altogether, the BetaShape code is now providing the same quantities as the LogFT code but also additional, detailed information using more reliable and more precise theoretical modellings for both beta and electron capture transitions. Its use in evaluations wills lead to improved nuclear data.

3. Results

We have compared the theoretical predictions based on the modelling described in previous section with precise measurements available in the literature. Most of these experimental values have already been presented in previous work (Mougeot, 2018). In addition, we have also considered:

i) the ε/β^+ ratio of the allowed decay between the ground state of ^{57}Ni and the third excited state of ^{57}Co at 1504.826 (21) keV, a weighted average of two values from (Konijn, 1958) and (Bakhru and Preiss, 1967);
ii) the ε/β^+ and K/β^+ ratios of the allowed decay between the ground state of ^{58}Co and the first excited state of ^{58}Fe at 810.7662(20) keV, which are weighted averages of six values for ε/β^+ which can be found in (Bé, 2016) and of three values for K/β^+ which can be found in (Bambynek, 1977);
iii) the K/β^+ ratio of the allowed decay between the ground state of ^{130}Cs and the ground state of ^{130}Xe from (Hagberg, 1981).

The latest Q-values from AME 2016 atomic mass evaluations (Wang, 2017) have been taken into account for all the calculations, as in our previous study.

Results are given in Table 1, with predictions from (Mougeot, 2018) and contribution of radiative corrections. In previous work, it was not possible to distinguish between the predictions using either Bahcall's or Vatai's approaches. In our present work, the use of more precise atomic wave functions has a significant influence. Indeed, Vatai's approach systematically leads to predictions closer to measurements than Bahcall's approach, and are thus preferred. This sounds reasonable as Vatai's approach relies on a better physical description of the overlap and exchange effects. It also highlights that our modelling has made a significant qualitative step forward, thanks to the inclusion of precise atomic energies and radiative corrections, reaching an overall consistency. However, Bahcall's approach is still considered to estimate the theoretical uncertainties, as detailed before in (Mougeot, 2018), because the sole propagation of energy uncertainties provides very small, unrealistic uncertainties on capture probabilities.

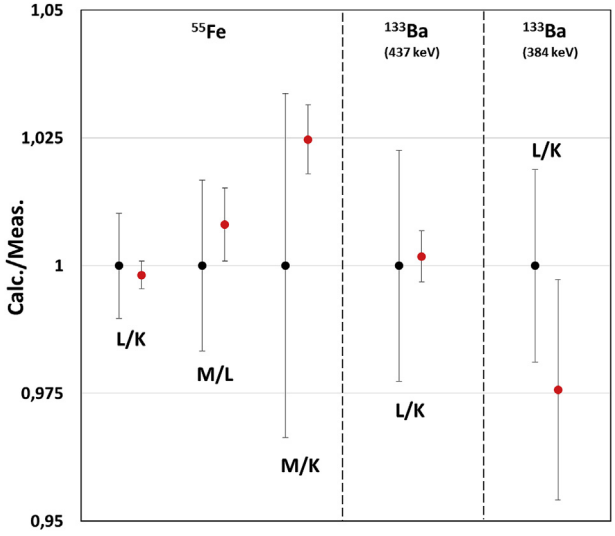

Fig. 2. Comparison of capture probability ratios for allowed transitions. Black points are ratios of the measured values and are given to shown the experimental uncertainties. Red points are ratios of calculated values to measured values, with theoretical uncertainties. (For interpretation of the references to colour in this figure legend, the reader is referred to the Web version of this article.)

These results are presented differently in Figs. 2–5 for a wide range of proton numbers and for allowed, first and second forbidden unique transitions. While it was not the case in previous work, we can clearly see that the present modelling provides predictions consistent with measurements, except in two cases. The first one is the ε/β^+ ratio in ^{22}Na decay which was already discussed in (Mougeot, 2018),

Table 1
Comparison between measured and calculated probability ratios from our previous work in (Mougeot, 2018) and from the present work. The contribution of the radiative correction for each ratio is given in the last column. The measured values are detailed in (Mougeot, 2018) or in the text.

Nuclide	Prob. ratio	Experiment	Previous work	This work	Rad. Corr.
Allowed					
^{11}C	K/β^+	0.00225 (15)	0.00218 (8)	0.00210 (6)	0.68%
^{22}Na	ε/β^+	0.1083 (9)	0.1143 (10)	0.1109 (9)	0.47%
	K/β^+	0.105 (9)	0.1058 (9)	0.1038 (8)	0.46%
^{55}Fe	L/K	0.1165 (12)	0.11823 (30)	0.11629 (31)	Negligible
	M/L	0.1556 (26)	0.1708 (12)	0.1568 (11)	Negligible
	M/K	0.0178 (6)	0.02019 (13)	0.01824 (12)	Negligible
^{57}Ni (1505 keV)	ε/β^+	1.460 (47)	n.a.	1.447 (11)	0.59%
^{58}Co (811 keV)	ε/β^+	5.61 (8)	n.a.	5.63 (8)	0.45%
	K/β^+	4.94 (6)	n.a.	4.98 (7)	0.44%
^{65}Zn	K/β^+	30.1 (5)	29.8 (6)	29.5 (7)	0.37%
^{133}Ba (437 keV)	L/K	0.371 (7)	0.375 (8)	0.362 (8)	Negligible
^{133}Ba (384 keV)	L/K	0.221 (5)	0.2265 (18)	0.2214 (11)	Negligible
^{130}Cs	K/β^+	1.025 (22)	1.077 (23)[a]	1.042 (19)	1.26%
First forbidden unique					
^{81}Kr	L/K	0.146 (5)	0.14851 (37)	0.14485 (33)	Negligible
^{84}Rb	K/β^+	1.12 (25)	0.905 (13)	0.909 (10)	1.13%
^{122}Sb	K/β^+	300 (50)	256 (10)	260 (10)	0.78%
^{126}I	K/β^+	20.2 (20)	20.38 (47)	20.55 (45)	0.88%
^{202}Tl	L/K	0.223 (18)	0.2105 (5)	0.2090 (6)	0.07%
^{204}Tl	L/K	0.47 (3)	0.5150 (49)	0.504 (5)	Negligible
Second forbidden unique					
^{138}La	L/K	0.391 (3)	0.416 (8)	0.403 (8)	Negligible
	M/K	0.102 (3)	0.1045 (24)	0.0996 (24)	Negligible
	M/L	0.261 (9)	0.251 (8)	0.247 (8)	Negligible
^{26}Al	ε/β^+	0.185 (44)	0.183 (10)	0.186 (12)	0.98%

[a] Calculated value given in (Hagberg, 1981) with a radiative correction of 1.3%.

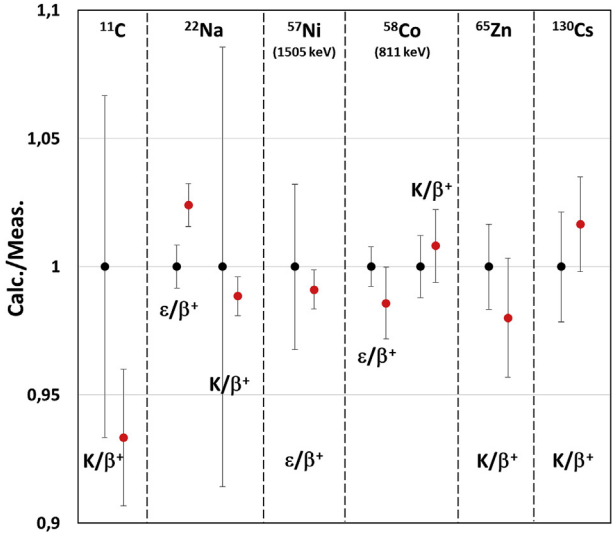

Fig. 3. Comparison of capture-to-positron ratios for allowed transitions. Black points are ratios of the measured values and are given to shown the experimental uncertainties. Red points are ratios of calculated values to measured values, with theoretical uncertainties. (For interpretation of the references to colour in this figure legend, the reader is referred to the Web version of this article.)

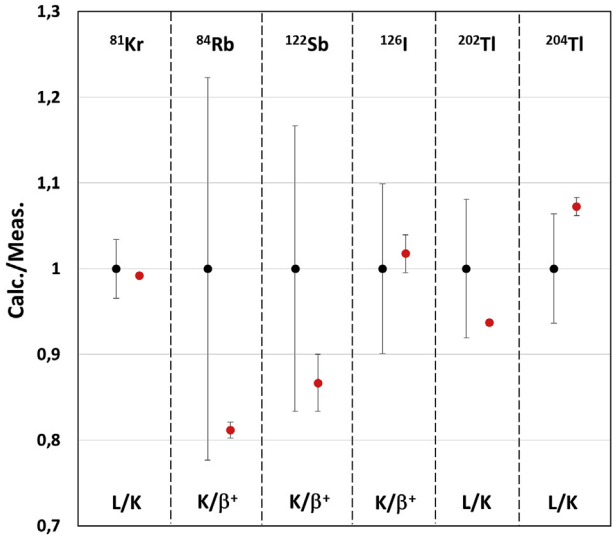

Fig. 4. Comparison of L/K and K/β^+ ratios for first forbidden unique transitions. Black points are ratios of the measured values and are given to shown the experimental uncertainties. Red points are ratios of calculated values to measured values, with theoretical uncertainties. (For interpretation of the references to colour in this figure legend, the reader is referred to the Web version of this article.)

highlighting the discrepancy of experimental data and stressing the need for a new high-precision measurement. However, it is noteworthy that the absolute difference – 0.0060 (13) before, 0.0026 (13) now – is reduced by more than a factor of two with the present result. The second one is the L/K ratio in ^{138}La decay, which measured value has a relative uncertainty less than 0.8%. Such a low uncertainty is definitely a challenge for any modelling. Again, the absolute difference – 0.025 (9) before, 0.012 (9) now – is reduced by more than a factor of two with the present result and is at the boundary of the statistical significance.

Finally, one can notice for certain transitions a difference of several percent between theory and experiment, even if the values are consistent when taking the uncertainties into account. Of course, this difference can be due to the precision of the measurement, some having a

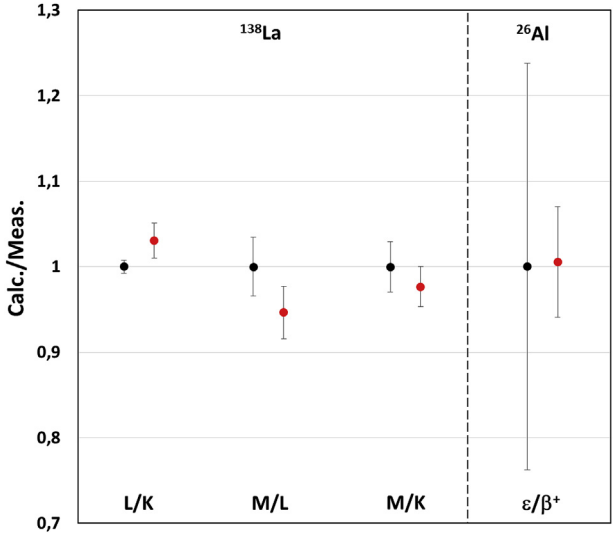

Fig. 5. Comparison of capture probability and ε/β^+ ratios for second forbidden unique transitions. Black points are ratios of the measured values and are given to shown the experimental uncertainties. Red points are ratios of calculated values to measured values, with theoretical uncertainties. (For interpretation of the references to colour in this figure legend, the reader is referred to the Web version of this article.)

large uncertainty. However, we would like to underline the high sensitivity of electron capture calculations to the accuracy of the energies used, both the atomic energies from the modelling and the input energies from the Q-values and nuclear levels. This fact could explain some of the remaining differences.

4. Contribution of the nuclear component

The low-energy transitions of interest in the present work occur through the weak interaction between two nuclear states, the initial one in the parent radionuclide and the final one in the daughter radionuclide. The coupling of the nuclear component and the lepton component is performed within the C_{κ_x} coefficients for electron captures, and within the theoretical shape factor $C(W)$ for beta plus transitions. In the present work, we have derived all the equations that are necessary to calculate these quantities following the Behrens and Bühring formalism (Behrens and Bühring, 1982). We are only giving below the equations required to reproduce the present results.

Essentially, every weak interaction process is described by a universal Hamiltonian density expressed in terms of self-interacting currents – a hadron current and a lepton current – and a multipole expansion is performed for both. This technique was applied in the past to describe electromagnetic transitions in nuclei because perfect knowledge of the electromagnetic interaction makes it favourable. In the present case, the structure of the weak interaction is only known empirically and particle physics experiments were used in the 1970s to select one of the many possible covariant forms, i.e. any linear combination of the scalar (S), pseud-scalar (P), vector (V), axial-vector (A) and tensor (T) components. We are considering in this work a pure (V-A) interaction, consistent with the Standard Model. In addition, the necessity of introducing a Coulomb field for the electrons leads to a very complicated formalism.

First, one can notice that the maximum energy of electron capture or beta transitions (less than 30 MeV) is negligible compared with the mass of the weak interaction bosons $W^{\pm}$ (about 80 GeV). This fact justifies the use of the Fermi effective theory which assumes an instantaneous point interaction between four particles. Second, the nucleon is assumed to feel only the weak interaction during the decay, the other nucleons within the nucleus are thus assumed to be spectators.

This assumption is called the impulse approximation and only measurements of very high precision could be sensitive to the neglected residual interactions.

After performing the multipole expansions and determining the transition matrices of beta and electron capture decays, Behrens and Bühring introduce specific quantities to express the C_{κ_x} coefficients as

$$C_{\kappa_x} = \sum_{K,\kappa_\nu} \left[M_K(k_x, k_\nu) + S_{\kappa_x} m_K(k_x, k_\nu)\right]^2 \tag{11}$$

and the theoretical shape factor as

$$C(W) = \sum_{K,\kappa_e,\kappa_\nu} \lambda_{k_e}\left[M_K^2(k_e, k_\nu) + m_K^2(k_e, k_\nu) - \frac{2\mu_{k_e}\gamma_{k_e}}{k_e W} M_K(k_e, k_\nu) m_K(k_e, k_\nu)\right]^2 \tag{12}$$

The M_K and m_K quantities are expressed by a sort of overlap between the nucleon and lepton wave functions. As the modelling assumes a spherical symmetry, one gets eventually a sum of radial integrals over some of the multipole expansion coefficients. A similar structure has been derived in both cases. For electron capture, we found:

$$\beta_{\kappa_x}\left[M_K(k_x, k_\nu) + S_{\kappa_x} m_K(k_x, k_\nu)\right] = \frac{\sqrt{2}}{\sqrt{2K+1}\sqrt{2J_i+1}} \sum_{L,s} \int_0^\infty \mathscr{A}_{KLs} r^2 dr \tag{13}$$

and for a beta transition:

$$M_K(k_e, k_\nu) = \frac{\sqrt{2}}{\sqrt{2K+1}\sqrt{2J_i+1}} \sum_{L,s} \int_0^\infty \mathscr{A}_{KLs} r^2 dr \tag{14}$$

The radial quantities $\mathscr{A}_{KLs}$ have been established to be:

- Time, non-relativistic vector component

$$^V\mathscr{A}_{KK0} = G_{KK0}(\kappa_f, \kappa_i) g_{\kappa_f}(r) F_{\text{lept.}}(r) g_{\kappa_i}(r) + S_{\kappa_f} S_{\kappa_i} G_{KK0}(-\kappa_f, -\kappa_i) f_{\kappa_f}(r) F_{\text{lept.}}(r) f_{\kappa_i}(r) \tag{15}$$

- Time, relativistic axial-vector component

$$^A\mathscr{A}_{KK0} = S_{\kappa_i} G_{KK0}(\kappa_f, -\kappa_i) g_{\kappa_f}(r) F_{\text{lept.}}(r) f_{\kappa_i}(r) + S_{\kappa_f} G_{KK0}(-\kappa_f, \kappa_i) f_{\kappa_f}(r) F_{\text{lept.}}(r) g_{\kappa_i}(r) \tag{16}$$

- Spatial, non-relativistic axial-vector component

$$^A\mathscr{A}_{KL1} = G_{KL1}(\kappa_f, \kappa_i) g_{\kappa_f}(r) F_{\text{lept.}}(r) g_{\kappa_i}(r) + S_{\kappa_f} S_{\kappa_i} G_{KL1}(-\kappa_f, -\kappa_i) f_{\kappa_f}(r) F_{\text{lept.}}(r) f_{\kappa_i}(r) \tag{17}$$

- Spatial, relativistic vector component

$$^V\mathscr{A}_{KL1} = S_{\kappa_i} G_{KL1}(\kappa_f, -\kappa_i) g_{\kappa_f}(r) F_{\text{lept.}}(r) f_{\kappa_i}(r) + S_{\kappa_f} G_{KL1}(-\kappa_f, \kappa_i) f_{\kappa_f}(r) F_{\text{lept.}}(r) g_{\kappa_i}(r) \tag{18}$$

The quantity $F_{\text{lept.}}(r)$ has been determined from lepton matrix elements. For electron capture, one gets:

$$F_{\text{lept.}}(r) = (-1)^{1-s} g_{\kappa_x}(r)\left[j_{k_\nu}(p_\nu r) G_{KLs}(\kappa_x, k_\nu) + j_{k_\nu-1}(p_\nu r) G_{KLs} S_{\kappa_x}(\kappa_x, -k_\nu)\right] + (-1)^{1-s} f_{\kappa_x}(r)\left[j_{k_\nu}(p_\nu r) G_{KLs}(-\kappa_x, k_\nu) + j_{k_\nu-1}(p_\nu r) G_{KLs}(-\kappa_x, -k_\nu)\right] \tag{19}$$

where $j_{k_\nu}(p_\nu r)$ is a spherical Bessel function, solution of the Dirac equation for the neutrino as a free particle. Similarly for beta plus decays, one gets:

$$F_{\text{lept.}}(r) = (-1)^{1-s} \frac{(p_e r)^{k_e-1}}{(2k_e-1)!!} H_{k_e}(r) \qquad \frac{(p_e r)^{k_e-1}}{(2k_e-1)!!}$$
$$\left[j_{k_\nu-1}(p_\nu r) G_{KLs}(-k_e, -k_\nu) + j_{k_\nu}(p_\nu r) G_{KLs}(-k_e, k_\nu)\right] - (-1)^{1-s} \frac{r}{R} D_{k_e}(r)\left[j_{k_\nu-1}(p_\nu r) G_{KLs}(k_e, -k_\nu) + j_{k_\nu}(p_\nu r) G_{KLs}(k_e, k_\nu)\right] \tag{20}$$

The quantities $H_{k_e}(r)$ and $D_{k_e}(r)$ are defined from the positron wave functions and similar quantities $h_{k_e}(r)$ and $d_{k_e}(r)$ exist, which replace the first ones in $F_{\text{lept.}}(r)$ for the m_K quantity:

$$\alpha_{k_e} \frac{(p_e r)^{k_e-1}}{(2k_e-1)!!}\left[H_{k_e}(r) + S_{\kappa_e} h_{k_e}(r)\right] = \begin{cases} f_{\kappa_e}(r) \text{ if } \kappa_e > 0 \\ g_{\kappa_e}(r) \text{ if } \kappa_e < 0 \end{cases} \tag{21}$$

$$S_{\kappa_e} \alpha_{k_e} \frac{(p_e r)^{k_e-1}}{(2k_e-1)!!} \frac{r}{R}\left[D_{k_e}(r) + S_{\kappa_e} d_{k_e}(r)\right] = \begin{cases} g_{\kappa_e}(r) \text{ if } \kappa_e > 0 \\ f_{\kappa_e}(r) \text{ if } \kappa_e < 0 \end{cases} \tag{22}$$

where α_{k_e} are the Coulomb amplitudes of the continuum positron wave functions and R is the nuclear radius.

Nucleon wave functions are then necessary to perform the calculations. Two simple models are considered in the present work, based on the mean field assumption. We first start by analysing the nuclear shell model to select the quantum numbers that will be assumed to define the nucleon wave function in accordance with the total angular momentum and parity of the nuclear state. We then calculate the wave function considering either a non-relativistic harmonic oscillator or a relativistic harmonic oscillator. The non-relativistic harmonic oscillator is well-known and we identify this radial wave function with the large relativistic component $g_\kappa(r)$. The small component $f_\kappa(r)$ was estimated by taking the non-relativistic limit of the Dirac radial equations:

$$f_\kappa(r) = \frac{1}{2M_N}\left(\frac{\mathrm{d}}{\mathrm{d}r} + \frac{\kappa+1}{r}\right) g_\kappa(r) \tag{23}$$

with M_N being the nucleon mass. In this case, it is not possible to treat separately neutrons and protons, which are thus considered as identical nucleons. For the relativistic harmonic oscillator, we have followed Strange in (Strange, 1998) to derive the most general analytical solutions. It is noteworthy that spin-orbit coupling naturally emerges from the Dirac equation as a relativistic effect, but this coupling is not sufficiently strong – by a factor of about 25 – to explain the well-known spin-orbit coupling in nuclear matter. However, in Strange's formulation this coupling is very much stronger (proportional to $1/\hbar$) than the real one in nuclear matter due to the way the harmonic oscillator is introduced in the Dirac equation. Finally, we have also considered the Coulomb potential from a uniform charged sphere which results in a shift in the oscillator strength, allowing us to treat neutrons and protons differently in this relativistic model.

The calculations in our study have been performed only for ground-state to ground-state transitions because of the difficulty to assign quantum numbers to nucleons for nuclear excited states with such simple nuclear models. The same oscillator strength has been considered to model the effect of the strong interaction as a mean nuclear potential, i.e. $\hbar\omega = 41\,A^{1/3}$ MeV, which is only expected to be good within an order of magnitude. The selected nucleon states are given in Table 2. Results for the probability ratios are given in Table 3.

We found that the results from non-relativistic harmonic oscillators are comparable or significantly better than those from relativistic harmonic oscillators. This is most probably due to the value of the oscillator strength, which can be found in nuclear shell model books and was derived from non-relativistic analysis of some basic nuclear properties. It is interesting to see a better agreement with measurements when including the nuclear component in some cases, e.g. ^{81}Kr, ^{130}Cs, ^{138}La and ^{202}Tl. It is a good indication that these nuclear states can be described with a single very dominant pure nucleon wave function, as long as it is not accidental – which is known to be the case for ^{138}La, this radionuclide exhibiting a special nuclear structure (Quarati, 2016). On the contrary, our nuclear models are clearly too simple to describe the

Table 2
Quantum states of the nucleons involved in the studied ground-state to ground-state transitions, selected by analysing the nuclear shell model.

Parent	J^π	State	Daughter	J^π	State
^{11}C	$3/2^-$	$\lvert p, 1p_{\frac{3}{2}}\rangle$	^{11}B	$3/2^-$	$\lvert n, 1p_{\frac{3}{2}}\rangle$
^{55}Fe	$3/2^-$	$\lvert p, 1f_{\frac{7}{2}}\rangle$	^{55}Mn	$5/2^-$	$\lvert n, 2p_{\frac{3}{2}}\rangle$
^{65}Zn	$5/2^-$	$\lvert p, 2p_{\frac{3}{2}}\rangle$	^{65}Cu	$3/2^-$	$\lvert n, 1f_{\frac{5}{2}}\rangle$
^{81}Kr	$7/2^+$	$\lvert p, 1f_{\frac{5}{2}}\rangle$	^{81}Br	$3/2^-$	$\lvert n, 1g_{\frac{9}{2}}\rangle$
^{122}Sb	2^-	$\lvert p, 1g_{\frac{7}{2}}\rangle$	^{122}Sn	0^+	$\lvert n, 1h_{\frac{11}{2}}\rangle$
^{126}I	2^-	$\lvert p, 1g_{\frac{7}{2}}\rangle$	^{126}Te	0^+	$\lvert n, 1h_{\frac{11}{2}}\rangle$
^{130}Cs	1^+	$\lvert p, 1g_{\frac{7}{2}}\rangle$	^{130}Xe	0^+	$\lvert n, 1g_{\frac{7}{2}}\rangle$
^{138}La	5^+	$\lvert p, 1g_{\frac{7}{2}}\rangle$	^{138}Ba	2^+	$\lvert n, 3s_{\frac{1}{2}}\rangle$
^{202}Tl	2^-	$\lvert p, 3s_{\frac{1}{2}}\rangle$	^{202}Hg	0^+	$\lvert n, 2f_{\frac{5}{2}}\rangle$
^{204}Tl	2^-	$\lvert p, 3s_{\frac{1}{2}}\rangle$	^{204}Hg	0^+	$\lvert n, 2f_{\frac{5}{2}}\rangle$

Table 3
Comparison between measured and calculated probability ratios. The calculations have been performed including the nuclear component involved in the electron capture transition, and in the beta plus transition where relevant. The nucleon wave functions have been determined from harmonic oscillators (HO), either non-relativistic or relativistic.

Nuclide	Prob. ratio	Experiment	Non-rel. HO	Rel. HO
^{11}C	K/β^+	0.00225 (15)	0.00209 (6)	0.00210 (6)
^{55}Fe	L/K	0.1165 (12)	0.12307 (33)	0.12213 (33)
	M/L	0.1556 (26)	0.1609 (11)	0.1577 (11)
	M/K	0.0178 (6)	0.01943 (13)	0.01927 (13)
^{65}Zn	K/β^+	30.1 (5)	660 (16)	0.328 (8)
^{81}Kr	L/K	0.146 (5)	0.14505 (33)	0.17185 (39)
^{122}Sb	K/β^+	300 (50)	250 (10)	26.8 (10)
^{126}I	K/β^+	20.2 (20)	19.76 (43)	0.913 (20)
^{130}Cs	K/β^+	1.025 (22)	1.011 (18)	0.817 (15)
^{138}La	L/K	0.391 (3)	0.393 (8)	0.335 (7)
	M/K	0.102 (3)	0.0990 (24)	0.0825 (20)
	M/L	0.261 (9)	0.252 (8)	0.246 (8)
^{202}Tl	L/K	0.223 (18)	0.2320 (7)	0.2773 (8)
^{204}Tl	L/K	0.47 (3)	0.661 (7)	2.874 (29)

^{65}Zn structure. In order to obtain high-precision predictions of electron capture probabilities, it would be necessary to consider accurate nuclear models which have to take account of realistic nuclear potentials, nucleon correlations, configuration mixing and deformation of the nucleus.

5. Conclusion

Starting from a previous study, we have improved our modelling of electron capture transitions considering precise atomic orbital energies – at the cost of a slight inconsistency in the atomic model – and radiative corrections. Comparison with available measurements has shown that the results from Bahcall's and Vatai's approaches for the overlap and exchange corrections, which were generalized to every subshell in previous work, can now be distinguished. As expected from a theory point of view, Vatai's approach leads to more accurate and more consistent results than Bahcall's one. We have also explored the influence of nuclear structure calculating the transition matrix elements which couple the lepton and nucleon wave functions. Using two simple nuclear models based on either non-relativistic or relativistic harmonic oscillators, we found that the predictions of electron capture probabilities are sensitive to the nuclear structure and, as expected, that a realistic nuclear model would be necessary to be conclusive.

We have thus demonstrated that high-precision calculation of electron capture decays requires an atomic model with electron correlations, radiative corrections especially for the capture-to-positron ratios, and accurate values of the input parameters i.e. Q-values and nuclear level energies. It is noteworthy that additional developments would be necessary regarding radiative corrections to reach the same precision level as for beta decays. The EMPIR project MetroMMC is addressing some of these challenges, e.g. the development of an accurate atomic code benchmarked with results from a multi-configurational Dirac-Fock code. We have also highlighted that high-precision measurements of electron captures have the potential to test the predictions of different nuclear structure models, and eventually to provide additional information.

Finally, we have improved the efficiency of our code, essentially through the tabulation of parameters to determine the atomic wave functions, and added the calculation of log*ft* values and splitting of the branch between capture and beta plus transitions. Doing this has allowed us to implement our modelling within the BetaShape code (http://www.lnhb.fr/rd-activities/spectrum-processing-software/), which is now able to calculate both beta and electron capture transitions with more accurate results than the LogFT code. In addition, BetaShape provides detailed information about beta and neutrino spectra, as well as about capture probabilities for every subshell. Its use is therefore recommended instead of LogFT during the evaluation procedure in order to improve the accuracy of nuclear decay data provided either by DDEP or NSDD networks.

Acknowledgment

This work was performed as part of the EMPIR Projects 15SIB10 MetroBeta and 17FUN02 MetroMMC. These projects have received funding from the EMPIR programme co-financed by the participating states and from the European Union's Horizon 2020 research and innovation programme.

References

Angeli, I., 1999. Table of Nuclear Root Mean Square Charge Radii. IAEA Report INDC(HUN)-033.
Bahcall, J.N., 1965. Exchange and overlap effects in electron capture ratios: physical basis and experimental tests. Nucl. Phys. 71, 267–272.
Bakhru, H., Preiss, I.L., 1967. Decay of Ni^{57} and excited levels in Co^{57}. Phys. Rev. 154, 1091.
Bambynek, W., Behrens, H., Chen, M.H., Crasemann, B., Fitzpatrick, M.L., Ledingham, K.W.D., Genz, H., Mutterer, M., Intemann, R.L., 1977. Orbital electron capture by the nucleus. Rev. Mod. Phys. 49, 77–221.
Bé, M.M., Chisté, V., Dulieu, C., Kellett, M.A., Mougeot, X., Arinc, A., Chechev, V.P., Kuzmenko, N.K., Kibédi, T., Luca, A., Nichols, A.L., 2016. Table of radionuclides. Monographie BIPM-5, vol. 5 Bureau International des Poids et Mesures 8 – A = 41 to 198.
Behrens, H., Bühring, W., 1982. Electron Radial Wave Functions and Nuclear Beta Decay. Clarendon, Oxford.
Crasemann, B., Chen, M.H., Briand, J.P., Chevallier, P., Chetioui, A., Tavernier, M., 1979. Atomic electron excitation probabilities during orbital electron capture by the nucleus. Phys. Rev. C 19, 1042–1046.
Desclaux, J.P., 1973. Relativistic Dirac-Fock expectation values for atoms with Z=1 to Z=120. Atomic Data Nucl. Data Tables 12, 311–406.
Gove, N.B., Martin, M.J., 1971. Log-f tables for beta decay. Nucl. Data Tables 10, 205–317.
Hagberg, E., Hardy, J.C., Jonson, B., Tidemand-Petersson, P., the ISOLDE Collaboration, 1981. A precise $P_K/P_{\beta+}$ measurement at Z=55 – (II). The decay of ^{130}Cs. Nucl. Phys. A 357, 365–380.
Holstein, B.R., 1979. Electromagnetic corrections to ε/β^+ ratios. Phys. Rev. C 20, 387.
Intemann, R.L., 1971. Angular distribution of internal bremsstrahlung in orbital-electron capture from polarized nuclei. Phys. Rev. C 3, 1.
Kellett, M.A., Bersillon, O., 2017. The decay data evaluation project (DDEP) and the JEFF-3.3 radioactive decay data library: combining international collaborative efforts on evaluated decay data. In: To Be Published in the Proceedings of the International

Conference on Nuclear Data for Science and Technology (ND2016), Bruges, Belgium, 11-16 September 2016.
Konijn, J., Van Nooijen, B., Hagedoorn, H.L., Wapstra, A.H., 1958. Branching ratios of electron capture to positon emission. Nucl. Phys. 9, 296–305.
Kotochigova, S., Levine, Z.H., Shirley, E.L., Stiles, M.D., Clark, C.W., 1997. Local-density-functional calculations of the energy of atoms. Phys. Rev. A 55, 191.
LogFT program, 2001. Gove and Martin. http://www.nndc.bnl.gov/nndcscr/ensdf_pgm/analysis/logft/. Original code from 1971.
Martin, P.C., Glauber, R.J., 1958. Relativistic theory of radiative orbital electron capture. Phys. Rev. 109, 1307.
Morrison, P., Schiff, L.I., 1940. Radiative K capture. Phys. Rev. 58, 24.
Mougeot, X., 2015. Reliability of usual assumptions in the calculation of β and ν spectra. Phys. Rev. C 91, 055504.
Mougeot, X., 2017. BetaShape: a new code for improved analytical calculations of beta spectra. EPJ Web Conf. 146, 12015.
Mougeot, X., 2018. Improved calculations of electron capture transitions for decay data and radionuclide metrology. Appl. Radiat. Isot. 134, 225–232.
Mougeot, X., Bisch, C., 2014. Consistent calculation of the screening and exchange effects in allowed β^- transitions. Phys. Rev. A 90, 012501.
NIST, 2009. Atomic reference data for electronic structure calculations. NIST Stand.Ref. Database 141. https://dx.doi.org/10.18434/T4ZP4F.
NNDC,Bhat, M.R., 2019. Evaluated nuclear structure data file (ENSDF). In: Qaim, S.M. (Ed.), Nucl. Data Sci. Tech. Springer-Verlag, Berlin, pp. 817. Data extracted using the NNDC On-Line Data Service from the ENSDF database, files revised as of February 2019. See. https://www.nndc.bnl.gov/ensdf/. http://www.nndc.bnl.gov/ensarchivals/.
Pálffy, A., 2010. Nuclear effects in atomic transitions. Contemp. Phys. 51, 471–496.
Quarati, F.G.A., Dorenbos, P., Mougeot, X., 2016. Experiments and theory of ^{138}La radioactive decay. Appl. Radiat. Isot. 109, 172–176.
Strange, P., 1998. Relativistic Quantum Mechanics with Applications in Condensed Matter and Atomic Physics. Cambridge University Press.
Towner, I.S., Hardy, J.C., 2008. Improved calculation of the isospin-symmetry-breaking corrections to superallowed Fermi β decay. Phys. Rev. C 77, 025501.
Vatai, E., 1970. On the exchange and overlap corrections in electron capture. Nucl. Phys. A 156, 541–552.
Wang, M., Audi, G., Kondev, F.G., Huang, W.J., Naimi, S., Xu, X., 2017. The AME2016 atomic mass evaluation. Chin. Phys. C 41, 03003.